Poisson's Ratios of Honeycomb-Structured Polymer Sheets Under Large Deformation

Dae-Yoon Kim, Namil Kim, Seok-Ho Hwang, Shiao-Wei Kuo, Jong-Hoon Lee, Sang-A Lee, Joong Hee Lee, Changwoon Nah,* Kwang-Un Jeong*

The mechanical properties of 2D honeycomb-structured polymer sheets (HSPS) are investigated with respect to the polar angle at large deformation. The tensile force fluctuates as an undamped negative sinusoidal wave with a periodicity of 15°. The amplitude of the fluctuation is proportional to the thickness of the HSPS, but the Young's modulus is independent of the thickness and the polar angle. Total and local Poisson's ratios of HSPS at the 30° polar angle are lower than those obtained at the 0° polar angle over the entire strain range, and the difference becomes smaller with increasing tensile strain. The experimentally observed structure–property relationship of the HSPS can provide important clues for understanding the deformation behavior of patterned polymeric materials.

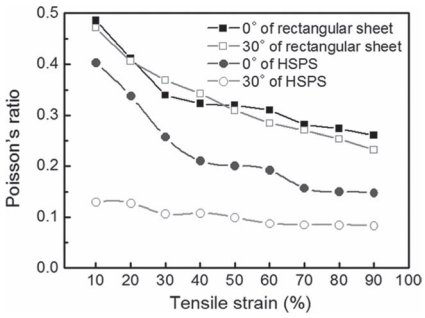

1. Introduction

Understanding the mechanical behavior of patterned polymeric materials at large deformation[1–11] is of significant importance for practical applications in smart membranes,[12] tunable photonic/phononic crystals,[13] adjustable microlenses,[14,15] and porous templates for cell culture.[16–23] Poisson's ratios (ν) at large deformations are relatively less understood compared to other mechanical properties.[24–27] On stretching solid materials, the cross-sectional areas often decrease because they resist volumetric change compared to their shape. The ν is defined as the ratio of a negative transverse strain ($-\varepsilon_t$) of the stretched material to its longitudinal strain (ε_l).[28] Since the interatomic bonds generally align along the stretching direction, most materials exhibit positive values, usually in the range of 0.25 and 0.35.[28] Poisson's ratio can also be described as a function of modulus $(3K - 2G)(6K + 2G)^{-1}$, where K and G stand for the bulk and the shear modulus, respectively.[28] When a material having a small G but a much higher K is stretched, it is much more difficult to change the volume compared to the shape. One of the extreme examples is an incompressible rubbery material ($\nu \approx 0.5$).[28,29]

When a transverse expansion occurs on stretching, ν becomes negative. A 2D honeycomb structure with an "inverted unit cell" is a representative example. The cross-sectional area of the stretched 2D honeycomb structure increases because of the unfolding of the inverted unit cell.[30–34] By introducing 3D microstructures with "inwardly bulging unit cells", a foam material with a negative ν can also be fabricated.[29–31] Similarly, by

D.-Y. Kim, J.-H. Lee, S.-A. Lee, J. H. Lee, C. Nah, K.-U. Jeong
Department of Polymer-Nano Science and Technology, Polymer Materials Fusion Research Center, Department of BIN Fusion Technology, Chonbuk National University, Jeonju, Jeonbuk 561-756, Korea
E-mail: cnah@jbnu.ac.kr; kujeong@jbnu.ac.kr
N. Kim
Department of Chemical and Biomolecular Engineering, Vanderbilt University, Nashville, TN 37235, USA
S.-H. Hwang
Department of Polymer Science and Engineering, Dankook University, Yongin 448-701, Korea
S.-W. Kuo
Department of Materials and Optoelectronic Science, Center for Nanoscience and Nanotechnology, National Sun Yat-Sen University, Kaohsiung, 804 Taiwan, Republic of China

DOI: 10.1002/macp.201100253

creating the reentrant structures on the molecular level, one can obtain a negative ν in polymers and composite laminates.[32,33] Since materials with a negative ν exhibit greater toughness and resistance than those with a positive one, they can be applied in knee pads, seat cushions, biomaterials, and air filters.[33–35]

In this research, the ν of 2D honeycomb-structured polymer sheets (HSPS) is investigated with respect to the polar angle. By varying the polar angle of HSPS from 0 to 30°, the tensile force at the 80% elongation is found to fluctuate with a wavelength of 15°. The amplitude of the undamped negative sinusoidal wave becomes larger in a thicker HSPS but its wavelength is not changed. Both total (ν_T) and local (ν_L) Poisson's ratios of HSPS at the 30° polar angle are lower than those at the 0° polar angle in the strain range of 10–90%. Based on the experimental results, it is concluded that the ν of HSPS depends on the polar angle.

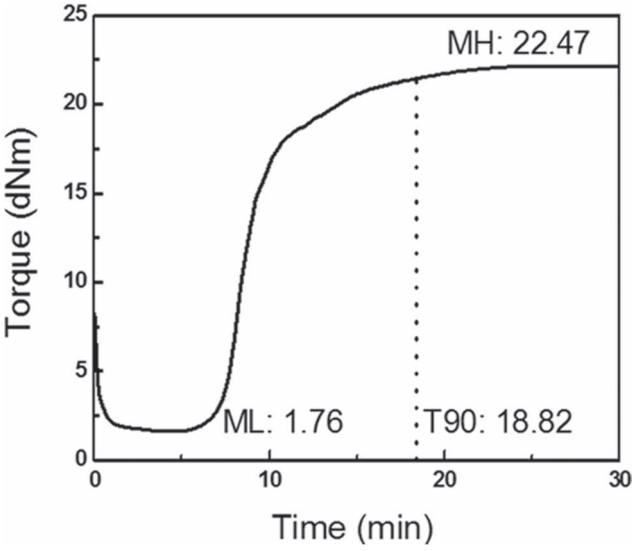

Figure 1. Optimized vulcanization time from the torque measurement by ODR-2000 at the programmed conditions (compression force = 25 tons, temperature = 160 °C and set-up time = 60 min).

2. Experimental Section

2.1. Materials

To fabricate the HSPS, acrylonitrile-butadiene rubber (NBR) provided by Kumho Petroleum Chemical Co. was used. It contained 34 wt% of acrylonitrile and exhibited a Mooney viscosity of 41 at 100 °C. The compounds were prepared based on ASTM D3182 and D3184 methods. For the vulcanization reaction, ZnO (Hanil Co.) and stearic acid (SA; Pyungwha Co.) were used. *N*-tert-Butyl-2-benzothiazylsulfenamide (TBBS; Bayer Co.) and sulfur (Seikwang Co.) were also added as a vulcanization accelerator and a curing agent, respectively.

2.2. Sample Preparation

The ingredients (NBR = 100 phr, ZnO = 5 phr, SA = 1 phr, TBBS = 1 phr, and S = 2 phr (phr = parts per hundred of rubber) were homogeneously mixed with a two-roll mill (Mixing roll M/C DS-1500R with a diameter of 304.8 mm) for 15 min and then dried at ambient temperature for 1 h. Based on the torque measurement using an oscillation disk rheometer (ODR-2000, Alpha technology) at the programmed conditions (compression force = 25 tons, temperature = 160 °C, and set-up time = 60 min), the optimum vulcanization time was estimated to be 20.6 min by considering the time at 90% delta torque (T90, min), and maximum (M_H) and minimum (M_L) torques (dNm), as shown in Figure 1. The NBR sheets were fabricated using a compression press (CMV50H-15-CLPX, CARVER Inc.) under a compression force of 25 tons.

The thicknesses of the NBR sheets were controlled from 0.5 to 2 mm by applying metal spacers between two compression plates. The NBR sheets were prepared with a geometric dimension of 72 mm × 92 mm × 1 mm. As shown in Figure 2a, to evaluate the edge effects of the rectangular-shaped samples, a dumbbell-shaped specimen was also prepared according to ASTM D412. In the rectangular-shaped samples, the shaded areas (72 mm × 10 mm) at the top and bottom represent the sample holding areas during the tensile test. In order to describe the sample geometry and the honeycomb structure, two different Cartesian coordinators were employed. One was

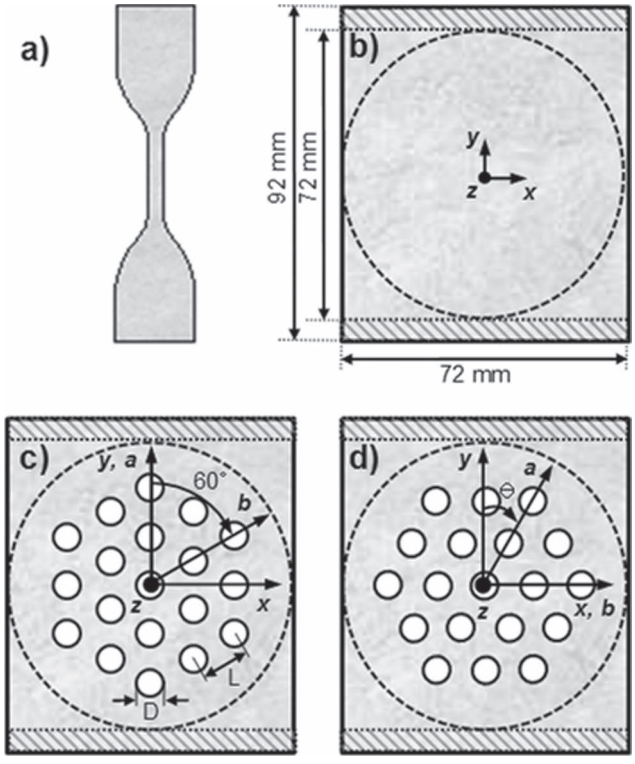

Figure 2. Schematic illustrations of specimens: a) ASTM D412 dumbbell-shaped specimen and rectangular-shaped specimen: b) without any holes and c,d) with 19 holes.

for the rectangular-shaped sample (*x*,*y*,*z*) and the other was for the 2D honeycomb structure (*a*,*b*). The *x*-axis and *y*-axis are the transverse and machinery directions, respectively, while the *z*-axis stands for the thickness direction. The rectangular-shaped samples were stretched along the *y*-axis (machinery direction) so that the stretched length along the *y*-axis indicates the elongation of the sample. In the 2D honeycomb structure, the *a*-axis is identical to the *b*-axis and the *r*-angle is 60°. As illustrated in Figure 2d, the polar angle is defined as the angle between the *y*-axis (machinery direction) and *a*-axis. When the polar angle is 0° (Figure 2c), the machinery direction (*y*-axis) is parallel to the apex of the honeycomb structure (*a*-axis), while a polar angle of 30° means that the machinery direction is parallel to the face of honeycomb structure ([11]-direction). Note that the *xyz* Cartesian coordinate does not change even though the honeycomb structure is rotated from a 0° (Figure 2c) to a 30° polar angle (Figure 2d). The 2D HSPS consisted of 19 holes with a diameter (*D*) of 6 mm. The distance (*L*) between centers of the neighboring six holes were controlled to be 12 mm, as illustrated in Figure 2c. Special attention was paid to minimize defects during the punching process. In addition, square meshes with a unit cell dimension of 3 mm × 3 mm were drawn on the in-plane (*xy*-plane) surface of the 2D HSPS for the in situ investigation of local deformations and stress concentrations.

2.3. Experiments with HSPS

Tensile tests were performed using a tensile tester (Long Travel Extensometer, LLOYD Instruments) at a cross-head speed of 50 mm s^{-1}. Laboratory designed T-shaped grips were used for holding the sample. The grips at the top and bottom held the shaded areas (72 mm × 10 mm) during the tensile test (Figure 2). A Nikon digital camera (COOLPIX S6) was used to monitor the deformation of the specimen. The total Poisson's ratio (ν_T) was obtained from the ratio of a negative transverse strain ($-\varepsilon_t$) of the stretched material to its longitudinal strain (ε_l), while the local Poisson's ratio (ν_L) was calculated from the ratio of a negative transverse strain [$-(\Delta x x_o^{-1})$] to its longitudinal strain [$(\Delta y y_o^{-1})$] of the center-to-center distance between the holes. Here, *x* and *y* are the distances in the transverse and machinery directions between the holes, respectively, and x_o and y_o are initial values before the deformation.

3. Results and Discussion

3.1. Tensile Properties of HSPS with Respect to the Sample Thickness

The tensile forces of the dumbbell-shaped specimen (ASTM D412) and the rectangular-shaped specimen without any holes are measured first at 80% elongation. As shown in Figure 3, the tensile force linearly increases with respect to the thickness, which means that the thickness itself does not generate the shape effect. The tensile forces of the rectangular-shaped specimen are much higher than those of the dumbbell-shaped specimen

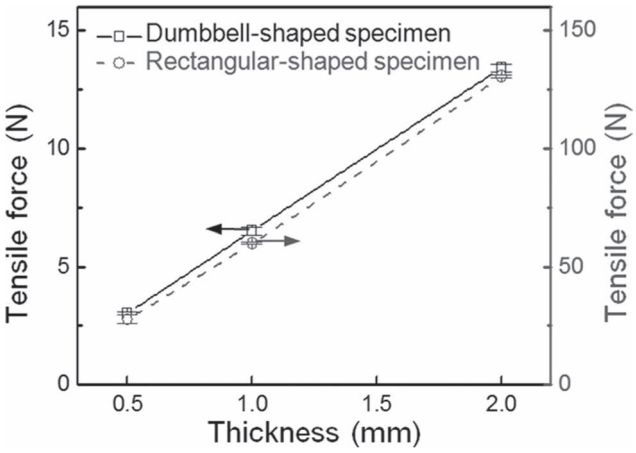

Figure 3. Comparison of tensile forces between ASTM D412 dumbbell-shaped specimen and rectangular-shaped specimen without any hole at 80% elongation with respect to the thickness from 0.5 to 2.0 mm.

because it is more difficult to stretch. Figure 4 illustrates the effect of the polar angle on the tensile force of the HSPS. Higher tensile forces are needed to stretch the thicker HSPS specimens. It should be noted that the tensile force fluctuates up and down like an undamped negative sinusoidal wave with a wavelength of 15°. However, the amplitude is reduced by decreasing the thickness of HSPS. This result indicates that the thicker HSPS samples are more sensitive to the polar angle, possibly because of the defects generated during the sample preparation and the stronger interfering corrections of the honeycomb structure. Since the cross-sectional area of the 2D HSPS is changed depending on the polar angle and the number of holes, the tensile force is used in the following discussion rather than the tensile stress.

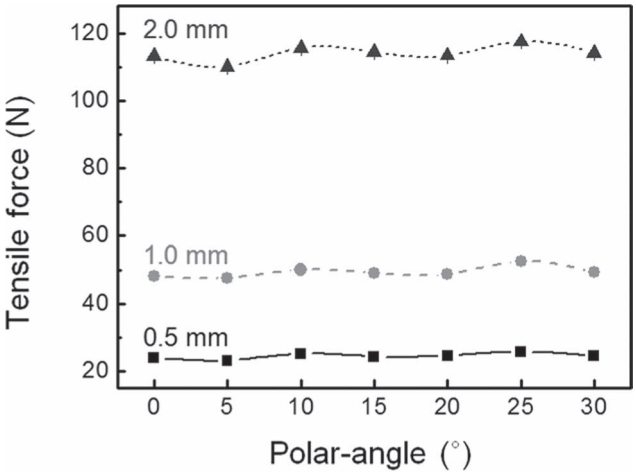

Figure 4. Tensile forces of HSPS with 19 holes at 80% elongation with respect to both the thickness from 0.5 to 2.0 mm and the polar angle from 0° to 30°.

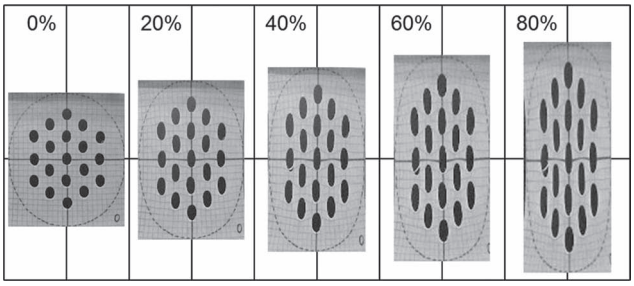

Figure 5. Photographs of HSPS with a 0° polar angle upon increasing the tensile strain from 0 to 80%.

The stress concentrations of the stretched HSPS are monitored using a digital camera at polar angles of 0° and 30°. For the in situ investigation, the square meshes with a unit cell of 3 mm × 3 mm are drawn on the in-plane (*xy*-plane) surface of HSPS. As shown in Figure 5 (polar angle = 0°) and Figure 6 (polar angle = 30°), the aspect ratios of the deformed holes increase with the tensile strain from 0 to 80%. It should be emphasized that the aspect ratios of the deformed holes increase upon moving away from the center and only the central holes maintain a C_{2v} symmetry. The holes in the machinery direction (*y*-axis in Figure 2c,d) reveal a C_2 symmetry, implying that the stress around the central hole is affected by the neighboring holes located not only on the *x*- and *y*-axes but also on the quadrant planes. As observed in a previous report,[8] it is found that the stress concentrations around the central holes decrease with the number of holes, which is more effective when the holes are arranged along the machinery direction. Therefore, to release and delocalize the concentrated stresses, we can purposely introduce defects around the stress-concentrated position. These simple tensile tests of HSPS can provide intuitive experimental pictures of the structure–property relationship of the patterned polymer architectures.

3.2. Young's Modulus of HSPS with Respect to the Polar Angle

The Young's modulus (E = 11.5 MPa) of the NBR sample measured from a weighing method[36,37] is well matched

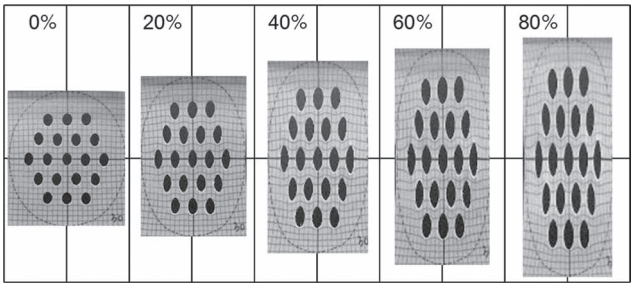

Figure 6. Photographs of HSPS with a 30° polar angle upon increasing the tensile strain from 0 to 80%.

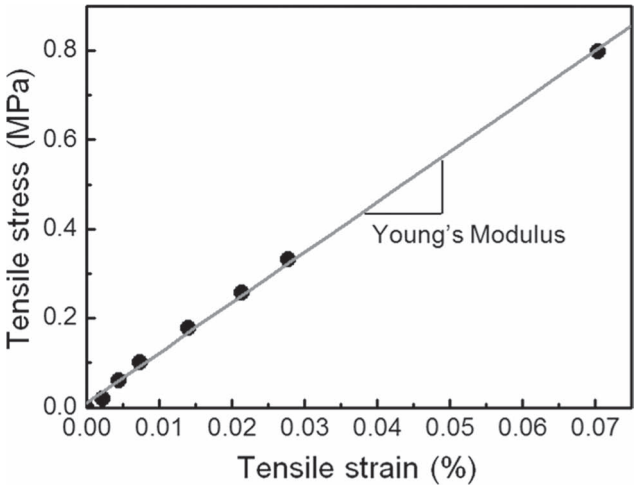

Figure 7. Stress–strain curve of the dumbbell-shaped specimen.

with the value (11.6 MPa) from the initial slope of the stress–strain curve obtained from a tensile tester (Figure 7). According to the Phantom model, the average crosslink density (n) and the number of structural units between cross-links (q) can be calculated to be 1561 mol m^{-3} and 11, respectively, where E and q are defined as $E = \sigma\varepsilon^{-1} = 3nRT$ and $q = \rho(M_m n)^{-1}$, respectively. Here, σ, ε, R, T, ρ, and M_m represent tensile stress, tensile strain, the universal gas constant, absolute temperature, density, and the molecular weight of the structural unit, respectively.

Young's moduli of HSPS at a thickness of 0.5, 1.0, and 2.0 mm are also measured with respect to the polar angle. The slopes of the stress–strain curves at the initial deformation remained constant within an error range (11.5 ± 0.5 MPa) regardless of the polar angle and sample thickness (Figure 8). It indicates that the Young's modulus, one of the intrinsic properties of materials, is not significantly

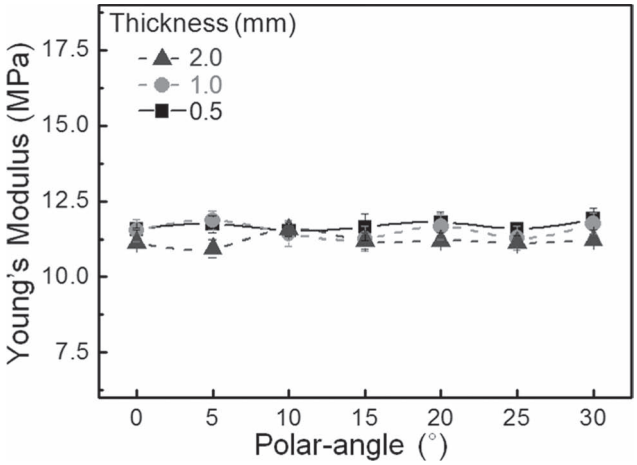

Figure 8. Young's modulus of HSPS in accordance with changing both the thickness from 0.5 to 2.0 mm and the polar angle from 0° to 30°.

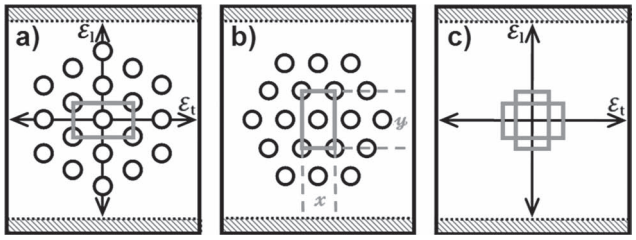

Figure 9. Schematic illustrations of HSPS with 19 holes at a) 0° and b) 30° polar angles, and c) the rectangular-shaped specimen without any holes. Here the Poisson's ratio is defined as the ratio of the transverse strain to the longitudinal strain.

dependent on the geometry of the sample. It seems that the properties of the rubber sheets at smaller deformations (below 10%), are not much affected by any defects around the holes and any changes in their hole shapes.

3.3. Total and Local Poisson's Ratios of HSPS

Most of the polymeric materials exhibit v in the range of 0 and 0.5. When the initial volume (V_o) is smaller than the volume (V_t) at a certain strain, the v is between 0 and 0.499. As the v is closer to 0, ε_l becomes larger than ε_t. A perfectly incompressible polymeric material ($V_o = V_t$) deformed elastically at a small strain shows $v \approx 0.5$. The geometries of HSPS at the polar angles of 0° and 30° are schematically illustrated in Figure 9a and b, respectively. Total Poisson's ratios ($v_T = -\varepsilon_t\varepsilon_l^{-1}$) of HSPS at large deformations are summarized in Figure 10. By increasing the tensile strain from 10 to 90%, the v_T of HSPS gradually decreases from 0.45 to 0.25 at a polar angle of 0° and from 0.40 to 0.16 at a polar angle of 30°, respectively. Compared with the v_T of the rectangular-shaped sheet without any hole (Figure 9c), the geometric edge effect is larger at the polar angle of 0° up to 30% elongation. The rectangular-shaped sheet without any holes shows $v_T \approx 0.3$ at small deformations, which is far from the values of the Poisson's ratio of a conventional unfilled rubber vulcanized sheet (≈0.5).[38] The disparity may be attributable to the square shape of the sheets used in this study. If the width (W, transverse direction) is large enough compared with the length of the sheet (L, machine direction), it is generally assumed to be at a pure shear condition.[39] For instance, the tensile extension causes almost all contraction in the thickness, not in the width, leading to the smaller values of Poisson's ratio close to 0.

Even though the v_T of HSPS is affected not only by the structure and the symmetry but also by the geometric edge effects, it does not give the local structure–property relationship of the patterned polymer architecture. Therefore, the local Poisson's ratio (v_L), representing a local volume change during its deformation, is also evaluated from $v_L = -(\Delta x x_o^{-1})(\Delta y y_o^{-1})^{-1}$, where x and y are the lengths in the transverse and machinery directions, respectively. From the v_L of rectangular-shaped sheets at the polar angles of 0° and 30° (Figure 11), it is recognized that the local geometries of the selected rectangles do not affect the v_L at the center of the HSPS so that it is safe to investigate the symmetry effect of HSPS at large deformations. Upon stretching the HSPS from 10 to 90%, the v_L of HSPS at the polar angle of 0° decreases with a similar pattern to the rectangular-shaped sheet even though the value is lower than that of the rectangular-shaped sheet (Figure 9a). On the other hand, the v_L of HSPS at the polar angle of 30° (Figure 9b) varies with the tensile strain and its value is much lower than that of HSPS at the polar angle of 0° (Figure 11). It means that the volume of HSPS at the polar angle of 30° is larger than that of HSPS at the

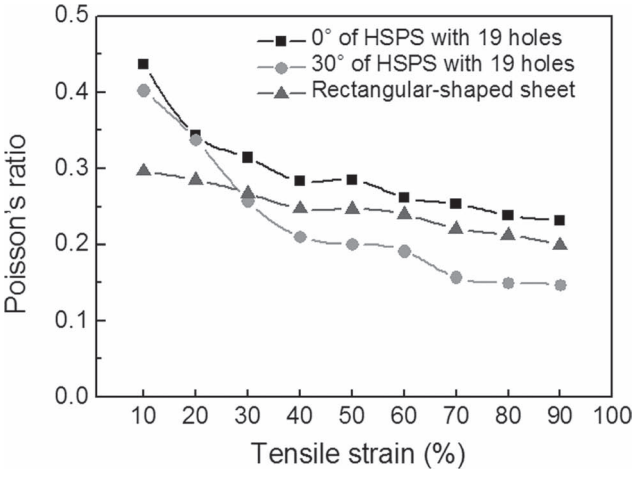

Figure 10. Total Poisson's ratio evaluated from the ratio of the negative transverse strain ($-\varepsilon_t$) of the stretched material to its longitudinal strain (ε_l).

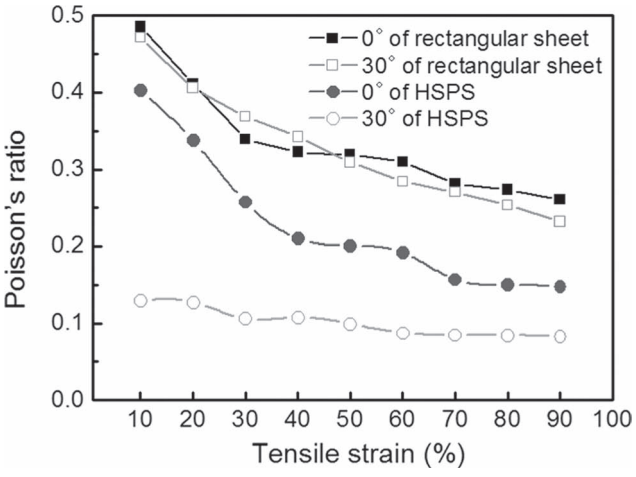

Figure 11. Local Poisson's ratio evaluated from the ratio of a negative transverse strain [$-(\Delta x/x_o)$] to its longitudinal strain [$(\Delta y/y_o)$] of the center-to-center distance between the holes.

polar angle of 0° and rapidly increases up to its limited value at a smaller deformation. This may be explained by the number of holes in the transverse and machinery directions. Note that holes aligned along the apex of HSPS are more effective in decreasing the tensile force and reducing the stress concentration than those located along the plane. For similar reasons, the HSPS having the smaller number of holes along the machinery direction shows a relatively lower contraction along the transverse direction, which leads to the lower Poisson's ratio at a large deformation.

4. Conclusion

The structure–property relationship of a patterned 2D HSPS was demonstrated with respect to the polar angle. By varying the polar angle from 0° to 30°, the tensile force of HSPS fluctuated like an undamped negative sinusoidal wave and the amplitude increased with the thickness. The Young's modulus of HSPS was almost independent of the thickness and the polar angle of HSPS. Total and local Poisson's ratios were monitored by stretching the HSPS along the 0° and 30° polar angle with a tensile strain from 10 to 90%. From the experimental results, it was realized that total and local Poisson's ratios of HSPS at the 30° polar angle are lower than those at the 0° polar angle. The structure–property relationship of the HSPS depending on its symmetrical polar angle and thickness can give insight into the application of a periodic patterned structure for tunable smart materials in the fields of optoelectronic devices and biochemical sensors.

Acknowledgements: This work was mainly supported by 1101000214 and 2011K000776 by the Korean government (Ministry of Education, Science and Technololgy) and C. N. acknowledges support from WCU-R33-2008-000-10016-0.

Received: April 29, 2011; Revised: July 11, 2011; Published online: September 7, 2011; DOI: 10.1002/macp.201100253

Keywords: honeycomb-structured polymer sheets; large deformations; mechanical properties; Poisson's ratios; structures

[1] Q. Z. Fang, T. J. Wang, H.-M. Li, *Polymer* **2006**, *47*, 5174.
[2] S. Singamaneni, K. Bertoldi, S. Chang, J.-H. Jang, S. L. Young, E. L. Thomas, M. C. Boyce, V. V. Tsukruk, *Adv. Funct. Mater.* **2009**, *19*, 1426.
[3] N. T. Qazvini, N. Mohammadi, *Polymer* **2005**, *46*, 9088.
[4] P. Jiang, J. F. Bertone, K. S. Hwang, V. L. Colvin, *Chem. Mater.* **1999**, *11*, 2132.
[5] Y. Xu, B. Zhu, Y. Xu, *Polymer* **2005**, *46*, 713.
[6] J.-S. Yu, S. Kang, S. B. Yoon, G. Chai, *J. Am. Chem. Soc.* **2002**, *124*, 9382.
[7] L. Li, Y. Zhong, C. Ma, J. Li, C. Chen, A. Zhang, D. Tang, S. Xie, Z. Ma, *Chem. Mater.* **2009**, *21*, 4977.
[8] K.-Y. Jin, D.-Y. Kim, S.-E. Kim, S.-W. Kuo, J. H. Lee, M.-Y. Lyu, S.-H. Hwang, A. N. Gent, C. Nah, K.-U. Jeong, *Macromol. Chem. Phys.* **2011**, *212*, 896.
[9] M. Hara, M. Bellinger, J. A. Sauer, *Polym. Int.* **1991**, *26*, 137.
[10] Y. Tian, C. Dai, H. Ding, Q. Jiao, L. Wang, Y. Shi, B. Liu, *Polym. Int.* **2007**, *56*, 834.
[11] R. J. Dai, G. H. Gao, H. X. Zhang, *Polym. Int.* **2010**, *59*, 738.
[12] N. Maruyama, T. Koito, J. Nishida, T. Sawadaishi, X. Cieren, K. Ijiro, O. Karthaus, M. Shimomura, *Thin Solid Films* **1998**, *327*, 854.
[13] H. Míguez, S. M. Yang, N. Tétreault, G. A. Ozin, *Adv. Mater.* **2002**, *14*, 1805.
[14] H. Ren, D. Ren, S.-T. Wu, *Opt. Express* **2009**, *17*, 24183.
[15] X. Huang, C.-M. Cheng, L. Wang, B. Wang, C.-C. Su, M.-S. Ho, P. R. LeDuc, Q. Lin, *Appl. Phys. Lett.* **2008**, *92*, 251904.
[16] S. H. Park, Y. Xia, *Adv. Mater.* **1998**, *10*, 1045.
[17] B. de Boer, U. Stalmach, H. Nijland, G. Hadziioannou, *Adv. Mater.* **2000**, *12*, 1581.
[18] C. X. Cheng, Y. Tian, Y. Q. Shi, R. P. Tang, F. Xi, *Langmuir* **2005**, *21*, 6576.
[19] A. Imhof, D. J. Pine, *Nature* **1997**, *389*, 948.
[20] M. Tanaka, M. Takebayashi, M. Shimonura, *Macromol. Symp.* **2009**, *279*, 175.
[21] J. B. Chaudhuri, M. G. Davidson, M. J. Ellis, M. D. Jones, X. J. Wu, *Macromol. Symp.* **2008**, *272*, 52.
[22] Y. Tian, H. Ding, Q. Jiao, Y. Shi, *Macromol. Chem. Phys.* **2006**, *207*, 545.
[23] Y. Tian, S. Liu, H. Ding, L. Wang, B. Liu, Y. Shi, *Macromol. Chem. Phys.* **2006**, *207*, 1998.
[24] N. Ravirala, A. Alderson, K. L. Alderson, *J. Mater. Sci.* **2007**, *42*, 7433.
[25] T. Kawamura, K. Urayama, S. Kohjiya, *Macromolecules* **2001**, *34*, 8252.
[26] C. C. Honeker, E. L. Thomas, R. J. Albalak, D. A. Hajduk, S. M. Gruner, M. C. Capel, *Macromolecules* **2000**, *33*, 9395.
[27] W. Ren, P. J. McMullan, A. C. Griffin, *Macromol. Chem. Phys.* **2008**, *209*, 1896.
[28] Y. C. Fung, *Foundations of Solid Mechanics*, Prentice-Hall, New Jersey, **1968**.
[29] S. W. Tsai, H. T. Hahn, *Introduction to Composite Materials*, Technomic, Pennsylvania, **1980**.
[30] S. Burns, *Science* **1987**, *238*, 551.
[31] R. S. Lakes, *Science* **1987**, *235*, 1038.
[32] T. L. Warren, *J. Appl. Phys.* **1990**, *67*, 7591.
[33] R. S. Lakes, *J. Mater. Sci.* **1991**, *26*, 2287.
[34] K. E. Evans, M. A. Nkansah, I. J. Hutchinson, S. C Rogers, *Nature* **1991**, *353*, 124.
[35] E. Bormashenko, A. Schechter, O. Stanevsky, T. Stein, S. Balter, A. Musin, Y. Bormashenko, R. Pogreb, Z. Barkay, D. Aurbach, *Macromol. Mater. Eng.* **2008**, *293*, 87.
[36] N. Koizumi, M. Kawahara, *Int. J. Numer. Anal. Meth. Geomech.* **2009**, *33*, 1513.
[37] Y.-P. Wu, Q.-X. Jia, D.-S. Yu, L.-Q. Zhang, *Polym. Test.* **2004**, *23*, 903.
[38] P. H. Mott, C. M. Roland, *Phys. Rev. B* **2009**, *80*, 132104.
[39] D. G. Young, *Tire Sci. Technol.* **1991**, *19*, 79.